Impact of the rhenium substitution on the oxygen evolution reaction of spinel CoFe$_2$O$_4$

Yuruo Zheng[12#], Ghulam Hussain[1#], Changcheng Zheng[1]; Xiaoqi Zhou[1]; Man Zhang[1]; Suirong Xie[1];

Qianhe Yin[1]; Shuyi Li[1], Batool Shanta[3], and Xiawa Wang[1*]

[1] *Division of Natural and Applied Sciences, Duke Kunshan University, Kunshan, Jiangsu 215316, China*

[2] *Department of Electrical & Computer Engineering, Pratt School of Engineering, Duke University,*

Durham, North Carolina 27708, United States

[3] *Department of Physics, and Key Laboratory of Strongly-Coupled Quantum Matter Physics (CAS),*

University of Science and Technology of China, Hefei, Anhui 230026, China

[*]email: xiawa.wang@dukekunshan.edu.cn

[#]Yuruo Zheng and Ghulam Hussain contributed equally to this work.

1. Computational Model

Density Functional Theory (DFT) calculations were used to investigate the detailed structural change brought by the doped rhenium atoms. In order to simplify the calculation, the simulation was done on bulk materials with the atom substitution on sites located at (Re atomic position: 0.747753005, 0.247696844, 0.747753002) for cobalt substitution at the octahedral site while (Re atomic position: 0.390884180, 0.390884180, 0.605204437) for iron substitution at the tetrahedral site within each unit cell [1]. However, one should realize that the simulation is not an exact replication of the experimental condition because the real doping levels are much smaller than a substitution level within every unit cell. In computation, Co-site sample has a doping ratio of 12.5% while the Fe-site doping has a doping ratio of 6.3%. The reason for this setup is that a computation with a small doping level is essentially too costly because a large unit cell will need to be established with many more atoms. The smaller unit cell bulk material computation can give enough evidences for the participation of dopants in the

Nevertheless, the computation results not only gave us indications for the effect of rhenium from the density of states, but also gave out simulation results such as the material bandgap, magnetic moment, etc. Because these properties are not directly related to the OER performances, we include them here in the supplementary in case needed. It can be observed

that the Co side doping has a higher bandgap energy than the zero doping. These values generally agree with the values reported in literature for doped cobalt ferrite, but are on the higher end. A possible explanation by Dileep *et al.* mentioned that the transition of the cations, i.e., variation in inversion index, can push the valence band and decrease the conduction band due to the crystal field splitting and variation of the spin state, which leads to a decrease of bandgap energy. This can explain the phenomenon that the theoretical values (fully inverse Co ferrite structure) of the bandgap are higher than the experimental results.

Table S1. Tetrahedral and octahedral vibrational frequencies (υ_1 and υ_2) and the theoretical optical band gap values (in eV) of the nanoparticles. The absorption bands shift to the higher energy side for the doped material.

Material	υ_1 (cm^{-1})	υ_2 (cm^{-1})	GGA+U (eV)
Non-doped	587.70	404.49	2.595
Co site doped	591.56	415.59	2.855
Fe site doped	589.63	411.25	2.651

2. Characterization Method

2.1 The morphology of the nanoparticles was verified by Scanning electrons microscopy.

Before and after the OER test, we presented the sample morphology. We observed agglomerations of all our samples, indicating the presence of surface reconstruction during the OER process. The samples all crystallized into micron-sized particles ranging from 300 nm to 1.5 μm. Taken $CoFe_2O_4$, and $Co_{0.95}Re_{0.05}Fe_2O_4$ as examples, their SEM images before and after the tests areas depicted i in Figure S1 for,. The formation of the nanoparticles consists of multiparticle aggregations. Before the OER test, the grains were well oriented. However, after the OER test, the grains had a tangled and irregular shape.
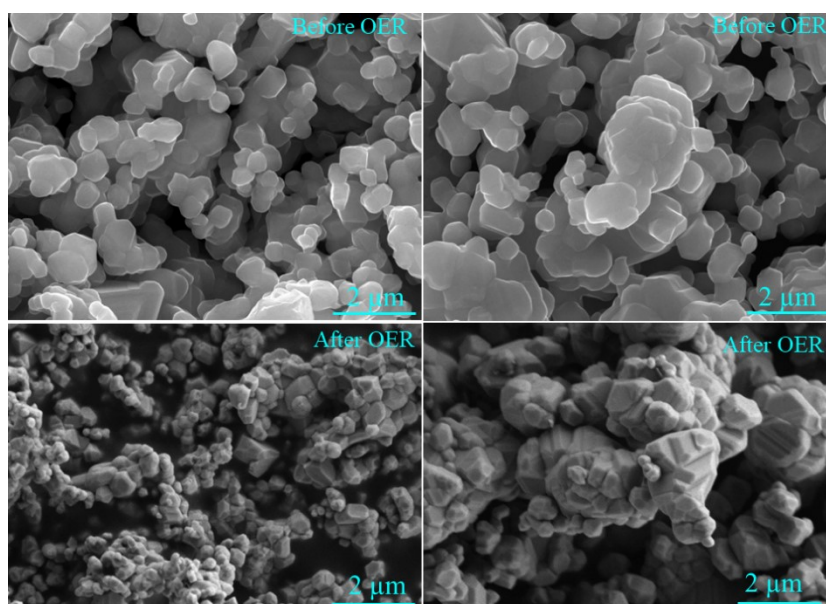
Figure S1. Before the OER test, the grains were well-oriented. However, after the OER test, the grains became tangled and had an irregular shape.

2.2 Room temperature vibrational spectroscopy analysis

In order to find the dominant factors that govern the properties of the catalysts, we used vibrational spectroscopy techniques, basically Fourier-transform infrared (FTIR) spectroscopy and Raman spectroscopy at room temperature plus Raman spectroscopy at low temperature to investigate the potential causes. The room temperature results have not given many differences for the three samples because of the small amount of doping. We presented the results here in case other researchers find them helpful.

The FTIR spectra of three samples ($CoFe_2O_4$, $Co_{0.95}Re_{0.05}Fe_2O_4$, and $CoFe_{1.95}Re_{0.05}O_4$) were recorded in the range of 400 to 4000 cm^{-1} at a temperature of 300 K, confirming the spinel structure in the Re-doped ferrite, as depicted in Figure S1. Notably, the spectra of the synthesized samples revealed the presence of two prominent absorption bands at approximately 500 – 650 cm^{-1} and 390 – 410 cm^{-1}, indicative of the cubic spinel structure associated with the intrinsic stretching vibrations of the metal-oxygen bond at the tetrahedral (Fe−O−Co) and octahedral (Fe−O− Fe) sites, respectively[3-5]. These absorption bands, tabulated in Table S1, serve as signatures of the inverse spinel phase of $CoFe_2O_4$. Additionally, it was observed that upon rhenium substitution, the absorption band broadened in the doped structure and slightly

shifted to higher frequencies, suggesting that the presence of rhenium induced distortion in the tetrahedral and octahedral sublattices. It is worth noting that significant bands around 1635 cm^{-1} and 3450 cm^{-1} correspond to the H–O–H bending modes of vibration and the O–H stretching attributed to adsorbed water molecules, respectively[2,7]. Furthermore, the vibrational frequencies of tetrahedral and octahedral sites in $Co_{1-z}Re_zFe_2O_4$ and $CoFe_{2-z}Re_zO_4$ (z = 0, 0.05) samples were utilized to calculate the force constant strength (Kt, Ko) of bonding between metal-oxygen bonds using Equations (1) and (2) [6,7].

$$K_O = 0.942128 \times \frac{M\upsilon_2^2}{M + 32} \qquad (1)$$

$$K_t = \sqrt{2} \times K_o\frac{\upsilon_1}{\upsilon_2} \qquad (2)$$

where M corresponds to the molecular weight of the samples, υ_1, and υ_2, refer to the vibrational frequency of tetrahedral and octahedral sites, respectively. The calculated force constant values are also enclosed in Table S1.
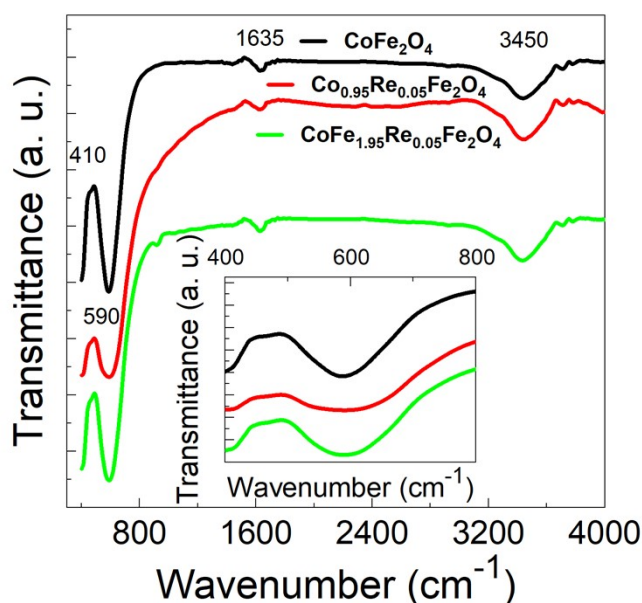

Figure S2. FTIR spectra of $CoFe_2O_4$, $Co_{0.95}Re_{0.05}Fe_2O_4$, and $CoFe_{1.95}Re_{0.05}O_4$ nanoparticles. Four absorption bands are marked at around 410, 590, 1635, and 3450 cm^{-1}. The inset shows the FTIR spectra within 400 – 800 cm^{-1}, and the Co-site doping spectra show a broadening behavior, indicating the influence of doping on the lattice.

2.3 Magnetic Analysis

The improved properties of Fe-site doping can also be observed with the materials' magnetic tests shown in Figure 2S (a-b). The field-dependent hysteresis loop (M-H) and temperature-dependent (M-T) magnetic curve at 4 K reveals that the samples exhibit a hard ferromagnetic behavior. The magnetic hysteresis (M-H) curve provides insights into various parameters such as saturation magnetization (M_s), anisotropy (K), remanence magnetization (M_r), and blocking temperature (T_B), as summarized in Table S2. The anisotropy is determined using equation 3[7].

$$K = \frac{H_c \times M_s}{0.98} \#(3)$$

Although the ZFC-FC magnetization curve exhibited spin-glass-like behavior across the entire temperature range, the extracted parameters have been significantly influenced by various factors. These include particle size resulting from the synthesis process and the presence of minute impurity substituents at the two interstitial A and B-sites of $CoFe_2O_4$. The behavior of saturation magnetization (M_s) and coercive field (H_c) can be attributed to factors such as particle size, defects, internal porosity (composition), magnetic moment, external defects (microstructural), and the preferred site occupancy of various ions. Almessiere *et al.* elucidated that magnetic parameters M_s and H_c could be linked to defects or porosity in the samples. Comparisons between Co-site doping and Fe-site substitution in $CoFe_2O_4$ revealed a decrease in M_s and M_r for Co-site doping and an increase for Fe-site substitution, which correlates closely with changes in particle grain size due to Re-substitution. Additionally, it's evident that at 4 K, the Re-substituted sample at the Co-site exhibits higher coercivity and significantly larger grain size, affirming the dominant role of surface morphology. The presence of interparticle exchange interaction in the sample suppresses H_c but significantly enhances M_r. Furthermore, Figure 2S(b) illustrates that the ZFC-FC magnetization curve tests of nanoparticles under 50 kOe displayed irreversible behavior with a blocking temperature of approximately 250 K, influenced by factors such as particle size distribution, magnetic anisotropy, and interparticle interactions. Moreover, based on Monte Carlo simulations, Ali *et al.* observed that increasing grain size markedly enhances coercivity and blocking temperature. However, strengthening the interparticle exchange interaction between particles suppresses H_c while enhancing M_r.
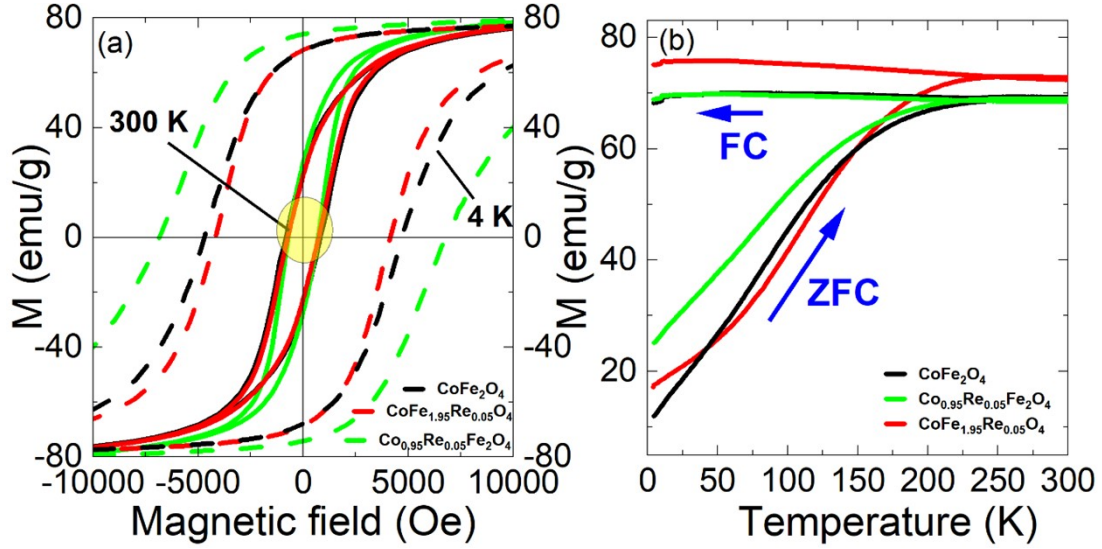
Figure S3. (a) Magnetic hysteresis loops of $CoFe_2O_4$, $Co_{1.95}Re_{0.05}Fe_2O_4$, and $CoFe_{1.95}Re_{0.05}O_4$ nanoparticles at 4 K (dash line) and 300 K (solid line), showing a variation of hysteresis shape with different sites of doping. (b) FC/ZFC curve of the three nanoparticles, indicating a spin-glass-like behavior of the nanoparticles.

Table S2. Magnetic parameters (M_s, M_r, H_c, K) of Re-doped nanoparticles were extracted at 300 K and 4 K. The magnetic parameters reduced for the Co-site doping while enhanced in Fe-site doping. The total magnetic moment and magnetization are obtained by theoretical calculation, showing a similar trend to the experimental results.

Samples	M_s (emu/g)		M_r (emu/g)		H_c (Oe)		K (erg/Oe)$\times 10^4$	
	300 K	4 K	300 K	4 K	300 K	4 K	300 K	4 K
Non-doped	80	80	26	68	817	4704	6.81	38.64
Co site doepd	78	77	18	66	735	4150	6.12	34.09
Fe site doped	81	83	27	75	712	6801	5.99	57.60

Table S3 presents the magnetic moment of individual atoms and the total magnetization derived from DFT calculations. Theoretical analysis reveals that the contribution of Re dopant to the total magnetization is insignificant, with the non-doped structure exhibiting the highest magnetic moment. However, experimental findings indicate that the Fe-site Re-doped structure exhibits marginally higher magnetization compared to the undoped structure. We attribute this disparity to the inversion degree, as previously reported. Specifically, the inversion degree in the doped nanoparticle is lower than that in the bulk structure, elucidating the observed increase in magnetization of the Fe-doped structure[8].

Table S3. The magnetic moment of individual atoms and total magnetization from DFT calculation.

Samples	Fe (μ_B)	Co (μ_B)	O (μ_B)	Re (μ_B)	Magnetization (μ_B / cell)
Non-doped	3.985	2.589	0.339	---	104
Co-site doping	3.735	2.475	0.300	0.596	96.00
Fe-site doping	3.812	2.449	0.317	0.191	96.97

References

[1] Ansari, S. M.; Sinha, B. B.; Phase, D.; Sen, D.; Sastry, P. U.; Kolekar, Y. D.; Ramana, C. V. Particle Size, Morphology, and Chemical Composition Controlled $CoFe_2O_4$ Nanoparticles with Tunable Magnetic Properties Via Oleic Acid Based Solvothermal Synthesis for Application in Electronic Devices. *ACS Appl. Nano Mater.* **2019**, *2*(4), 1828-1843.

[2] Shakil, M.; Inayat, U.; Arshad, M.; Nabi, G.; Khalid, N.; Tariq, N.; Shah, A.; Iqbal, M. Influence of Zinc and Cadmium Co-doping on Optical and Magnetic Properties of Cobalt Ferrites. *Ceram. Int.* **2020**, *46*(6), 7767-7773.

[3] Patil, S. A.; Mahajan, V. C.; Ghatage, A. K.; Lotke, S. D. Structure and Magnetic Properties of Cd and Ti/Si Substituted Cobalt Ferrites. *Mater. Chem. Phys.* **1998**, *57*(1), 86-91.

[4] Pradeep, A.; Chandrasekaran, G. FTIR Study of Ni, Cu and Zn Substituted Nano-particles of $MgFe_2O_4$. *Mater. Lett.* **2006**, *60*(3), 371-374.

[5] Labde, B. K.; Sable, M. C.; Shamkuwar, N. R. Structural and Infra-red Studies of $Ni_{1+x}Pb_xFe_{2-2x}O_4$ System. *Mater. Lett.* **2003**, *57*(11), 1651-1655.

[6] Sawant, S.; Suryavanshi, S. Iono-covalent and Yafet Kittle (YK) Angle Studies of Slow Cooled and Quenched CuZn-system. *J. Curr. Sci.* **1988**, *57*, 644-647.

[7] Khatun, N.; Ahmed, S.; Hossain, M. S.; Farhad, S. F. U.; Al-Mamun, M.; Alam, M. S.; Begum, M. H. A.; Tanvir, N. I.; Hakim, M.; Islam, S. Influence of Y^{3+} and La^{3+} Ions on the Structural, Magnetic, Electrical, and Optical Properties of Cobalt Ferrite Nanoparticles. *Heliyon* **2023**, *9*(2), e13019.

[8] Atif, M.; Hasanain, S.; Nadeem, M. Magnetization of Sol–gel Prepared Zinc Ferrite Nanoparticles: Effects of Inversion and Particle Size. *Solid State Commun.* **2006**, *138*(8), 416-421.